Heliyon 10 (2024) e29657

Contents lists available at ScienceDirect

Heliyon

journal homepage: www.cell.com/heliyon

Research article

CO_2 capture using silica-immobilized dicationic ionic liquids with magnetic and non-magnetic properties

Evandro Duarte [a,b], Franciele Bernard [b], Leonardo Moreira Dos Santos [b], Barbara B. Polesso [a,b], Rafael Duczinski [a,b], Vitor Forneck [b], Julian Geshev [c], Sandra Einloft [a,b,*]

[a] Post-Graduation Program in Materials Engineering and Technology, Pontifical Catholic University of Rio Grande do Sul – PUC, RS, Brazil
[b] School of Technology, Pontifical Catholic University of Rio Grande do Sul – PUC, RS, Brazil
[c] Institute of Physics, Federal University of Rio Grande do Sul, Porto Alegre, RS, Brazil

ARTICLE INFO

Keywords:
CO_2 capture
Mesoporous silica supports
Dicationic ionic liquid
Magnetic dicationic ionic liquids

ABSTRACT

The need to find alternative materials to replace aqueous amine solutions for the capture of CO_2 in post-combustion technologies is pressing. This study assesses the CO_2 sorption capacity and CO_2/N_2 selectivity of three dicationic ionic liquids with distinct anions immobilized in commercial mesoporous silica support (SBA- 15). The samples were characterized by UART-FTIR, NMR, Raman, FESEM, TEM, TGA, Magnetometry (VSM), BET and BJH. The highest CO_2 sorption capacity and CO_2/N_2 selectivity were obtained for sample SBA@DIL_2$FeCl_4$ [at 1 bar and 25 °C; 57.31 (±0.02) mg CO_2/g; 12.27 (±0.72) mg CO_2/g]. The results were compared to pristine SBA-15 and revealed a similar sorption capacity, indicating that the IL has no impact on the CO_2 sorption capacity of silica. On the other hand, selectivity was improved by approximately 3.8 times, demonstrating the affinity of the ionic liquid for the CO_2 molecule. The material underwent multiple sorption/desorption cycles and proved to be stable and a promising option for use in industrial CO_2 capture processes.

1. Introduction

Greenhouse gas (GHG) emissions are a growing concern, primarily due to high anthropogenic emissions from the burning of coal, natural gas, and oil [1]. The increase in the greenhouse effect has environmental, social, and economic impacts. Humanity is already experiencing the rising of land and ocean temperatures, resulting in more frequent cyclones, floods, heat waves, droughts, forest fires, dust storms, and desertification [2,3]. The main gases contributing to the increase in the greenhouse effect are carbon dioxide (CO_2), responsible for 75 % of emissions, methane (CH_4) 17 %, nitrous oxide (N_2O) 6 %, and fluorinated gases 2 % [4]. Energy production and industry are responsible for about 64 % of CO_2 emissions [5].

CO_2 emissions have increased by more than 50 % since the beginning of the industrial era and reaching a global record of 421 ppm in May 2022 [6]. The increase in atmospheric CO_2 concentration is responsible for two-thirds of the total energy imbalance, leading to a rise in the temperature of the planet [7]. A portfolio of options is available to mitigate CO_2 concentrations in the atmosphere. CO_2

* Corresponding author. Post-Graduation Program in Materials Engineering and Technology, Pontifical Catholic University of Rio Grande do Sul – PUC, RS, Brazil.
E-mail address: einloft@pucrs.br (S. Einloft).

https://doi.org/10.1016/j.heliyon.2024.e29657
Received 7 November 2023; Received in revised form 6 March 2024; Accepted 11 April 2024
Available online 15 April 2024

capture and storage (CCS) is one of the most promising technologies to mitigate CO_2 emissions from industry and power plants. The main drawback of CCS is the high cost of the capture step [8]. In the Carbon Capture and Utilization (CCU) process, CO_2 is captured and used as raw material to produce fuels and chemicals [9]. To mitigate CO_2 emissions, a capture step can be inserted in the existing pre-combustion, oxy-combustion and post-combustion processes. In post-combustion, the capture step can be easily adapted to existing power plants without the need for radical changes, obtaining high efficiency in the carbon capture process [10], removing CO_2 after the burning of the fossil fuel [11].

Chemical absorption by amine aqueous solutions is the benchmark technology for CO_2 capture [12], with a high absorption capacity, fast reaction kinetics, and low cost [13]. However, some drawbacks are considered, such as the high energy requirement for the solvent regeneration process, the corrosivity of the equipment, and the high degradability, making the process more expensive [14].

Aiming to overcome the problems related to the use of amines in CO_2 capture, other technologies are studied and applied, such as polymer-based membranes [15–17] and adsorbents, mainly zeolites [18–20], silicas [21–23] and activated carbon [24–26]. Adsorbent materials are good candidates for carbon capture processes, due to their porosity, high specific surface area, besides the competitive advantages related to the low energy consumption in the regeneration process, fast adsorption kinetics, non-corrosivity and good regenerability in the adsorption/desorption process. In general, solid adsorbents have low selectivity to CO_2 [27–29]. Higher selectivity can be achieved by supporting CO_2 selective molecules in solid support [30].

Ionic liquids (ILs) are formed by organic cations and organic or inorganic anions. The myriad of available anions and cations allows for a large number of combinations and the design of ILs with desired properties [31]. It is well known from the literature that ILs are selective for CO_2 [32]. Immobilization of ILs in solid supports can improve the affinity for CO_2, in addition to solving the drawbacks of ILs related to the high viscosity and low adsorption kinetics. The formation of thin ILs films in the solid supports enhances the mass transfer process [33].

The application of dicationic ionic liquids (DIL) and tricationic ionic liquids (TIL) is being investigated in various research fields, such as extraction [34], liquid chromatography [35], catalysis [36] and gas separation [37]. Multicationic ILs are seen as a potential alternative that could enhance the functionality of ILs, compared to traditional monocationics [38–40].

When an IL contains metal, such as transition metals or rare earth ions, in the anion, it is called a magnetic ionic liquid (MIL) [41]. These materials possess the properties of ionic liquids and the ability to respond magnetically to an external field, making them magneto-responsive materials [42]. The viscosity of MILs could decrease when subjected to an external magnetic field, which is a crucial characteristic for their use in gas separation processes [43].

The synthesis and immobilization of three imidazolium-based dicationic ionic liquids on a commercial silica support were described in this study. A polyethyleneglycol chain was used to connect the cations and different anions. CO_2 sorption capacity and CO_2/N_2 selectivity were evaluated for all samples and compared to the monocationic ILs described in the literature.

2. Experimental

2.1. Materiais

Triethylene glycol (TEG, ≥99.0 %, Sigma-Aldrich, China), sodium p-toluenesulfonate (TsOCl, ≥98.0 %, Sigma-Aldrich, China), potassium hydroxide (KOH, ≥85 %, VETEC, Brazil), (3-Chloropropyl) triethoxysilane (CPTES, ≥95.0 %, Sigma-Aldrich, U.S.A), imidazole (≥99.0 %, Sigma-Aldrich, Germany), iron (III) chloride ($FeCl_3$, ≥97.0 %, Sigma-Aldrich, Germany), lithium bis(trimethylsilyl)amide ($LiNTf_2$, ≥99.0 %, Sigma-Aldrich, China), SBA-15 (≥99.0 %, Sigma-Aldrich, China), pellets of sodium hydroxide (NaOH, ≥95.0 %, Sigma-Aldrich, U.S.A), magnesium sulfate ($MgSO_4$, ≥98.0 %, VETEC, Brazil), toluene (≥99.0 %, VETEC, Germany), dichloromethane (CH_2Cl_2, P.A, Synth, Brazil), chloroform ($CHCl_3$, P.A, Synth, Brazil) and acetonitrile (CH_3CN, ≥99.0 %, Merck, U.S.A). The organic solvents were previously purified prior to the reactions.

2.2. Syntheses of dicationic IONIC liquids

2.2.1. Synthesis of triethylene glycol di(p-Toluenesulfonate) (TsOTEGTsO)

Synthesis was performed following the procedure described in the literature [44]. In a round bottom flask, a solution of 16.55 g of TEG in 80 mL of dichloromethane was added to 53.60 g of TsOCl at room temperature. This mixture was cooled to 0 °C, then 58.20 g of KOH was added, in portions, and the reaction was stirred for 10 min, then allowed to warm to room temperature and kept under stirring for 12 h obtaining a heterogeneous solution. 50 mL of deionized water was added, diluting the previously formed white solid (TsOTEGTsO). The product was then extracted with chloroform, dried with magnesium sulfate, filtered and kept under vacuum, yielding 88 %. A schematic representation of the reaction synthesis is presented in Fig. 1. Characterizations are in agreement with the literature [44]. ^{1}H RMN ($CDCl_3$, 400 MHz, δ em ppm): 2.46 (6H, s, CH_3), 3.67 (4H, t, OCH_2CH_2O), 3.54 (4H, s, CH_2), 4.15 (4H, t, CH_2),

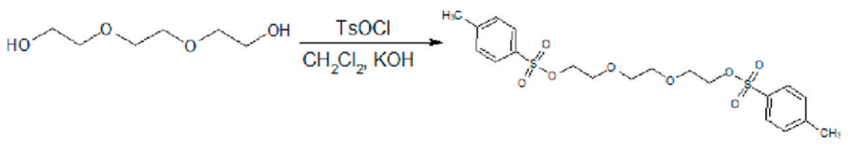

Fig. 1. Schematic representation of the synthesis of TsOTEGTsO.

7.35 (4H, d, CH), 7.81 (4H, d, CH). 13C RMN ($CDCl_3$, 400 MHz, δ em ppm): 21.62 (2C, s, -$\underline{C}H_3$), 68.75 (2C, s, S–*O*–$\underline{C}H_2$–$\underline{C}H_2$–O), 69.21 (2C, s, S–*O*–CH_2–$\underline{C}H_2$–O), 70.68 (2C, s, O–$\underline{C}H_2$–$\underline{C}H_2$–O), 127.95 (4C, s, $\underline{C}H_{arom.}$), 129.86 (4C, s, $\underline{C}H_{arom.}$), 133.03 (2C, s, $\underline{C}H_{arom.}$), 144.86 (2C, s, $\underline{C}H_{arom.}$).

2.2.2. Synthesis of 1,8-diimidazole-3,6-dioxaoctane (ImTEGIm)

Synthesis was performed following the procedures described elsewhere [45]. In a three-neck flask, 13.07 g of imidazole was melted at approximately 100 °C and then 6.98 g of NaOH was added. After complete dissolution, 50 mL of dry toluene was added to form an azeotropic mixture with the water generated by the reaction, stirred for 3 h, and the toluene/water mixture was removed under vacuum. To the imidazole sodium obtained, 40 g of TsOTEGTsO diluted in 100 mL of acetonitrile was added and refluxed for 24 h. The solvent was removed by simple distillation and the remaining product in the flask was washed in dichloromethane separating Im TEGIm and sodium *p*-toluenesulfonate. The liquid extracted with dichloromethane was washed with deionized water, and the aqueous solution was kept under vacuum under heating at 60 °C to remove the solvent, remaining only a viscous liquid of light brown color, yielding 73 %. The schematic representation is given in Fig. 2. The characterizations are in agreement with the literature [44,45]. 1H RMN (D_2O, 400 MHz, δ em ppm): 3.51(4H, s, $C\underline{H}_2$), 3.66 (4H, t, $OC\underline{H}_2C\underline{H}_2O$), 4,07 (4H, t, $C\underline{H}_2$), 6.95 (4H, d, $C\underline{H}$), 7.51 (2H, s, $C\underline{H}$). 13C RMN ($CDCl_3$, 400 MHz, δ em ppm): 46.81 (1C, d, N–$\underline{C}H_2$– CH_2–O), 68.30 (1C, d, N–$CH_2\underline{C}H_2$–O), 69.69 (2C, q, $O\underline{C}H_2\underline{C}H_2O$),120.35 (2C, d, -$\underline{C}H$═CH-), 129.43 (2C, s, –CH═$\underline{C}H$-), 138.13 (2C, s, N–$\underline{C}H$═N).

2.2.3. Synthesis of dichlorate 1,8-diimidazole-3,6-dioxaoctane-bis- (propyl)triethoxysilane (DIL_2Cl)

The experimental procedure was performed according to the literature [46]. 7.10 g of ImTEGIm, 20 mL of dry toluene and 14.06 g of CPTES (added slowly under an inert medium) were added in a three-neck flask. The mixture was then stirred for 24 h at 65 °C. After completion, two phases appeared, attributed to DIL_2Cl and toluene. DIL_2Cl was cleaned with anhydrous toluene and evaporated under vacuum, resulting in a highly viscous liquid with a yield of 87 %. The illustration of the synthesis process can be viewed in Fig. 3, and the results of the characterizations match the findings previously documented in the literature [44–46]. 1H RMN (D_2O, 400 MHz, δ em ppm): 0.60 (2H, s, -*Si*-$C\underline{H}_2$-CH_2-), 1.97 (t, 4H, -*Si*–CH_2–$C\underline{H}_2$-CH_2-), 2.39 (s, 12H, CH_3–$C\underline{H}_2$–*O*–Si-), 3.59 (s, 9H, $C\underline{H}_3$–CH_2–*O*–Si-), 3.63 (t, 8H, -$CH_2C\underline{H}_2OC\underline{H}_2C\underline{H}_2OC\underline{H}_2$ CH_2-), 3.78 (t, 4H, N–$C\underline{H}_2$–CH_2-), 4.21 (q, 2H, -*Si*–CH_2–CH_2-$C\underline{H}_2$-N-), 7.07 (d, 1H, -N-CH═$C\underline{H}$–N-), 7.20 (d, 1H, -N-$C\underline{H}$═CH–N-), 7.70 (s, 1H, -N-$C\underline{H}$═N-). 13C RMN (D_2O, 400 MHz, δ em ppm): 8.40 (2C, d, O–Si–$\underline{C}H_2$–CH_2–CH_2–N), 20.52 (6C, s, $\underline{C}H_2$–CH_2–*O*–Si), 23.39 (6C, s, CH_2–$\underline{C}H_2$–*O*–Si), 46.81 (2C, d, O–Si–CH_2–$\underline{C}H_2$–CH_2–N), 49.15 (2C, q, O–Si–CH_2–CH_2–$\underline{C}H_2$–N), 51.67 (2C, t, N–$\underline{C}H_2$–CH_2–O), 68.35 (2C, d, N–CH_2– $\underline{C}H_2$–O), 69.63 (2C, s, O–$\underline{C}H_2$–$\underline{C}H_2$–O), 120.46 (2C, d, N–$\underline{C}H$═CH–N), 129.43 (2C, s, N–CH═$\underline{C}H$–N), 137.95 (2C, d, N–$\underline{C}H$═N).

2.3. Chemical immobilization OF IONIC liquids in solid supports and anions exchange

The procedure for immobilization of 10 % DIL_2Cl on solid support (SBA-15) was based on the literature [47]. The solid support was previously dried in an oven at 110 °C for 2 h. Then 1.55 g was weighed directly into a three-neck flask and 30 mL of dry toluene was added and the mixture was stirred at room temperature for 2 h. 0.17 g of DIL_2Cl was diluted in 5 mL of deionized water and added in toluene at 95 °C and kept for 24 h, in a reflux system, producing the SBA@DIL_2Cl, as seen in Fig. 4.

The SBA@DIL_2Cl anion exchange reaction (Fig. 5) was performed according to a procedure adapted from the literature [48,49]. The mixture of $LiNTf_2$ salt (in 50 mL of distilled water) and immobilized DIL_2Cl (2:1 ratio) was stirred at room temperature for 78 h. Subsequently, the mixture was filtered, repeatedly washed with deionized water, and extracted with soxhlet using first deionized water and dichloromethane, which removed the unreacted products and produced SBA@DIL_2NTf_2.

To obtain $FeCl_4^-$ as an anion, $FeCl_3$ (dissolved in acetonitrile) and DIL_2Cl (2:1) were added to SBA@DIL_2Cl and stirred in an inert medium at 60 °C for 48 h, obtaining SBA@DIL_2$FeCl_4$. The product was filtered, washed with deionized water and soxhlet extracted with deionized water to remove unreacted products.

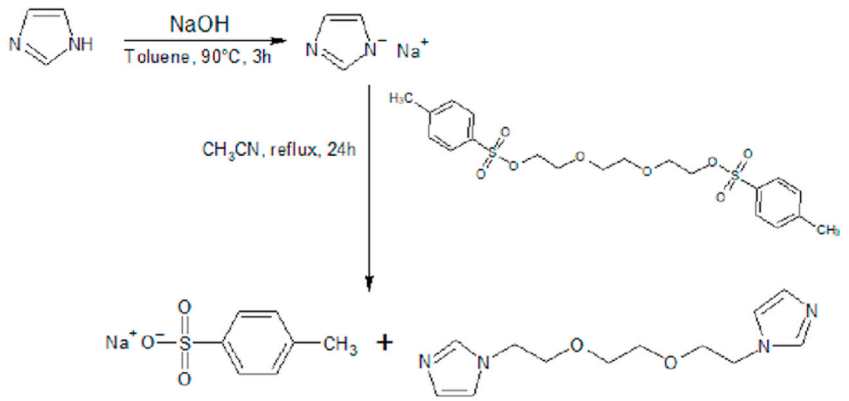

Fig. 2. Schematic representation of the synthesis of ImTEGIm.

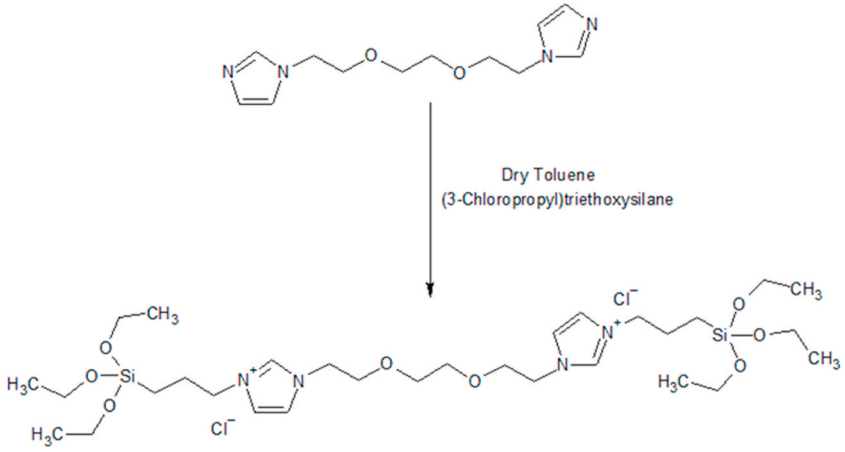

Fig. 3. Schematic representation of the synthesis of DIL_2Cl.

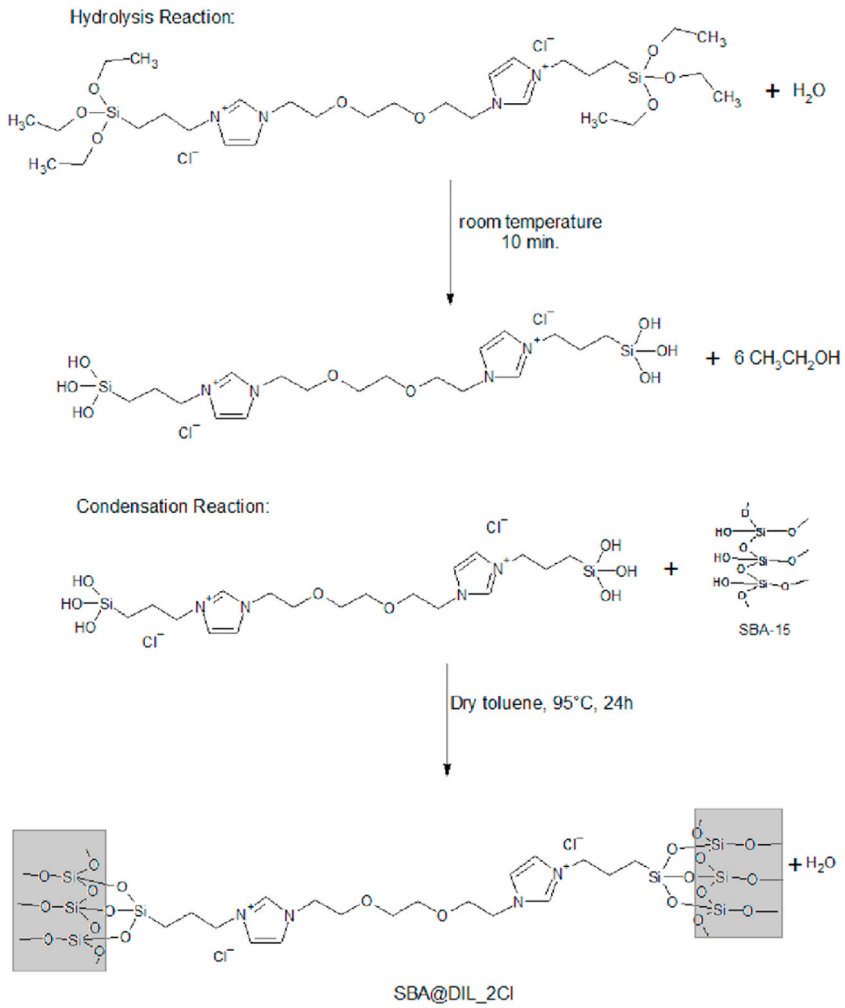

Fig. 4. Schematic representation of the synthesis of hydrolysis and condensation of DIL_2Cl for immobilization on the adsorbent support, forming SBA@DIL_2Cl.

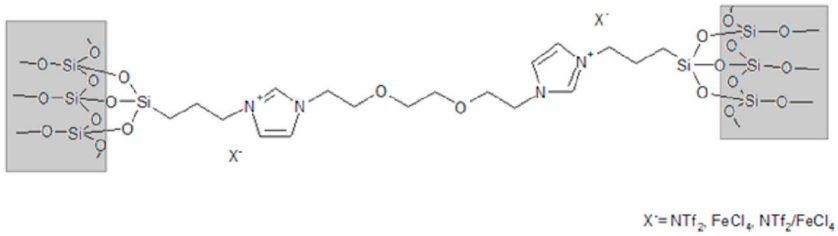

Fig. 5. Anion exchange of the SBA@DIL_2Cl for SBA@DIL_2NTf$_2$, SBA@DIL_2NTf$_2$/FeCl$_4$ and SBA@DIL_2FeCl$_4$.

To obtain a DIL containing FeCl$_4$/NTf$_2$ as an anion, a partial exchange was first performed with the LiNTf$_2$ salt, in a 1:1 ratio with the SBA@DIL_2Cl, following the same procedures reported above to obtain the NTf$_2$ anion. The remaining chloride anions were exchanged for the $FeCl_4^-$ anionic complex, using the same procedure described before, except for FeCl$_3$: SBA@DIL_2Cl ratio (1:1) obtains SBA@ DIL_NTf$_2$/FeCl$_4$.

2.4. Samples characterization

The structures of the dicationic ionic liquids (DILs) were analyzed using a range of techniques. An infrared spectrometer, FTIR PerkinElmer Spectrum One, with a Universal Attenuated Total Reflectance sensor (UATR-FTIR) was used for the analysis. Additionally, a Bruker Advance DRX-400 spectrometer operating at 400 MHz was used to perform the 1H and 13C NMR analyses in the liquid state and the ^{29}Si MAS-NMR in the solid state. The Brunauer-Emmett-Taller (BET) method was used to analyze the specific surface area, and the Barrett-Joyner-Halenda (BJH) method was used to determine the pores volumes and sizes, with the aid of the Quantachrome equipment New - Surface Area & Pore Size Analyzer. To determine the thermal stability and the percentage of DIL and magnetic dicationic ionic liquid (MDIL) grafted onto the support, a thermogravimetric analysis (TGA) was performed under a nitrogen atmosphere between 25 and 800 °C and a heating rate of 20 °C/min, using TA Instruments Discovery SDT 650. Equation 1: IL % = $[(W_{167}–W_{800})/W_{167}] \times 100$ was used to calculate the actual percentage of IL grafted on the support, where W_{167} and W_{800} are the sample weights at 167 °C and 800 °C, respectively [50]. To gain further insight into the mesopore materials, a range of microscopy techniques were utilized. The Field Emission Scanning Electron Microscope (FESEM) was used, with the FEI Inspect F50 equipment in secondary electron mode (SE), to perform microscopy analyses. The hexagonal structures of the support with and without DILs were confirmed using transmission electron microscopy (TEM) with aTecnai G2 T20 FEI equipment operating at 200 kV. The anionic iron

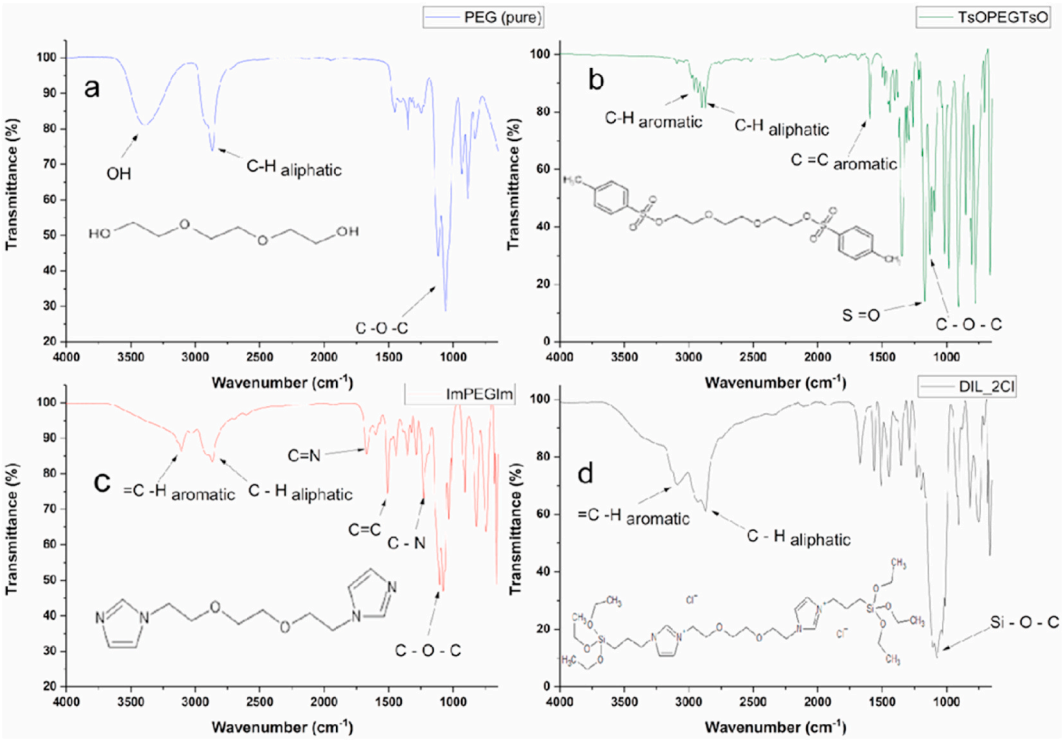

Fig. 6. FT-IR spectra of a) TEG (pure), b) TsOTEGTsO, c) Im TEGIm, d) DIL_2Cl.

complexes contained in the supports were characterized using Raman spectroscopy, which was performed with a Horibam LabRamHr Evolution Laser Raman Spectrometer, model DXR (laser excitation wavelength of 532 nm), and Access alpha 300 (632.8 nm - micro-Raman single-spot analysis and mapping microscope). Finally, the magnetic properties were analyzed using a Vibrant Sample Magnetometer (VSM), model EZ9 by MicroSense, to evaluate the impact of an external magnetic field on the samples.

2.5. CO_2 sorption measurements

The CO_2 sorption capacity was determined using the pressure decay method, as described in the literature [51]. The experiment was carried out three times to ensure accuracy. The sample, which weights approximately 0.6 g, was dried in an oven at 80 °C for 1.5 h prior to the test. The CO_2 sorption tests were carried out at 25 °C and the amount of adsorbed CO_2 was calculated using the method described in our previous works [52,53].

2.6. CO_2/N_2 selectivity tests

Selectivity experiments were carried out at 25 °C and 20 bar in a dual-chamber gas sorption cell based on Koros et al. [51] using a binary mixture (15.89 mol % of CO_2 and a balance of N_2). Gas chromatography with a thermal conductivity detector was used to determine the composition at the exit of the sorption system, obtaining the non-adsorbed CO_2/N_2 fraction. To calculate the separation efficiency, the procedure described in the literature was followed [52,54]. The molar fractions were determined in the gas phase (Yi) and the sample phase (Xi) according to equation (2):

$$S = \frac{XCO2/YCO2}{XN2/YN2} \tag{2}$$

3. Results and discussion

3.1. Precursors and IONIC liquids characterization

The IR spectra in Fig. 6 provide valuable information about the molecular structure of the synthesized molecules, confirming the success of the synthesis and supporting the NMR results. In Fig. 6a, TEG, the starting molecule of the reaction, shows characteristic absorption of O–H stretching bands (3388 cm^{-1}), aliphatic C–H stretching (2925 - 2869 cm^{-1}), folding of aliphatic C–H (1455 - 1351 cm^{-1}), and C–*O*–C stretching of ether group (1116 and 1056.9 cm^{-1}) [46]. Fig. 6b presents the TsOTEGTsO spectrum that presents characteristic band vibrations of aromatic C–H elongation (2959 - 2929 cm^{-1}), C═C aromatic (1596 - 1348 cm^{-1}) and aliphatic S═O elongation (1169 cm^{-1}), indicating the presence of the *p*-toluenesulfonate group [55]. The aliphatic C–H elongation band (2899 - 2872 cm^{-1}), and the stretching C–*O*–C of the ether group (1133–1092 cm^{-1}) are alsoobserved. The disappearance of the O–H stretching indicates the formation of TsOTEGTsO (3388 cm^{-1}).

From Fig. 6C, one can see the typical imidazolium bands that replace the *p*-toluenesulfonate. Aromatic = C–H elongation (3111

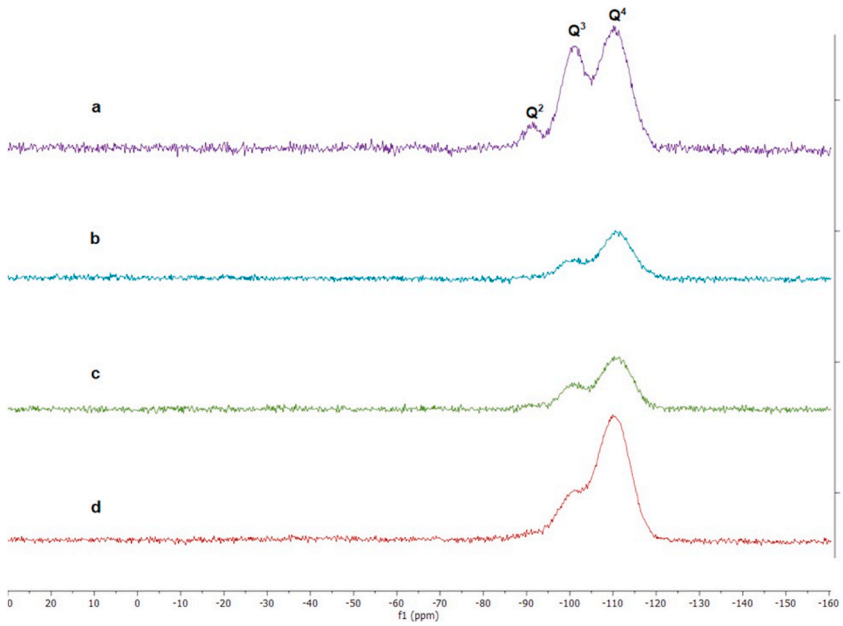

Fig. 7. ^{29}Si MAS-NMR spectra of a) SBA-15 (pure), b) SBA@DIL_2NTf_2 10 %, c) SBA@DIL_NTf_2/$FeCl_4$ 10 %, d) SBA@DIL_2$FeCl_4$ 10 %.

cm^{-1}), aliphatic C–H elongation (2911 - 2869 cm^{-1}), C═N elongation (1673 cm^{-1}), C═C elongation (1506–1440.5 cm^{-1}) and C–N elongation (1229 cm^{-1}). Also, the characteristic band of the C–*O*–C of TEG is maintained (1077 cm^{-1}).

Fig. 6d, after CTPES addition in ImTEGIm an intense band characteristic of Si–*O*–C (1035 cm^{-1}) and Si–C elongation (817 cm^{-1}) can be seen, confirming the obtainment of DIL_2Cl.

3.2. *Supported dicationic IONIC liquids - characterization*

The immobilization of the ionic liquid on the SBA-15 mesoporous support was evaluated by ^{29}Si MAS-NMR (Fig. 7). The pristine mesoporous silica (Fig. 7a) spectra show three typical resonance frequencies at −110 ppm, - 100 ppm and −92 ppm, assigned to [Si $(OSi)_4$] (Q^4), [Si $(OSi)_3$ OH] (Q^3) and [Si$(OSi)_2$ $(OH)_2$] (Q^2) groups of the SBA-15. After immobilization of the DILs [10 % (w/w)] (see Fig. 7 b, c and d) a reduction in the bands Q^2, Q^3 and Q^4 was observed, indicating the reaction of SBA-15 hydroxyl groups with the silane groups present in the DILs that confirms the immobilization of the DIL in the solid support.

Fig. 8 presents the ^{29}Si MAS-RMN spectra for a sample with 20 % of DIL immobilized in SBA-15. This sample with a higher DIL content was synthesized to improve the signal related to IL and confirm the immobilization of DIL. A reduction in Q^2 and Q^3 bands and the appearance of T^1 and T^3 bands (bands at −48 ppm and −68 ppm attributed to [R–Si (OSi) $(OH)_2$] (T^1) and [R–Si $(OSi)_3$] (T^3) suggest that DIL has reacted with the hydroxyl groups of the SBA-15 and formed a covalent bond with the mesoporous material [56].

Fig. 9 show the results of the TGA analysis of pristine SBA-15, DILs. And MDILs that were immobilized in the solid support. All of the samples exhibited a first stage of mass loss between 25 and 82 °C attributed to the moisture adsorbed by hygroscopic SBA-15 [57]. Pristine SBA-15 showed a more significant mass loss compared to the supports with immobilized DILs or MDILs. This behavior is probably associated with the filling of pores and the presence of ILs on solid surfaces reducing the availability of hydroxyl groups and inhibiting the presence of moisture [58]. The second stage of mass loss is related to the silane ligands present on the surface of the support, starting at around 167 °C for all three samples containing DILs. The third stage of mass loss is associated with less accessible organic fragments remaining from DlLs and can be used to calculate the percentage of DIL and MDIL grafted to the support [59,60]. The mass loss of SBA@DIL_2NTf_2, SBA@DIL_2$FeCl_4$ and SBA@DIL_NTf_2/$FeCl_4$ was 11.3 %, 9.9 % and 11.6 %, respectively, confirming that the immobilized DIL content is closely in agreement with the theoretical value of 10 %.

The specific surface areas of the pristine SBA-15, DILs and MDILs grafted on SBA-15 were determined by the Brunauer-Emmett-Teller (BET) method (Fig. 10). The results showed that pristine SBA-15 (Fig. 10a) has type IV isotherms and a type H1 hysteresis loop, which are characteristic of regular cylindrical pores and a high degree of uniformity of pore size, a typical feature of mesoporous materials [61]. The supports SBA@DIL_2$FeCl_4$ (Fig. 10c), SBA@DIL_2NTf_2 (Fig. 10b) and SBA@DIL_NTf_2/$FeCl_4$ (Fig. 10d) showed type IV isotherms and a type H3 hysteresis loop, which is related to the presence of open and partially blocked mesopores due to the addition of DILs and MDILs.

It can be observed that samples containing the NTf_2^- anion resulted in a more pronounced change in the hysteresis loops due to the anion size. The NTf_2^- molecule is larger than that of $FeCl_4^-$, thus filling the pores more extensively and generating greater difficulty in filling with N_2 during the test, as also described by Sing and coworkers [62]. The highest specific surface area was observed for SBA-15 (777 m^2/g), which then decreased with the immobilization of DILs and MDILs [SAB@DIL_2$FeCl_4$ (347 m^2/g), SAB@DIL_NTf_2/$FeCl_4$

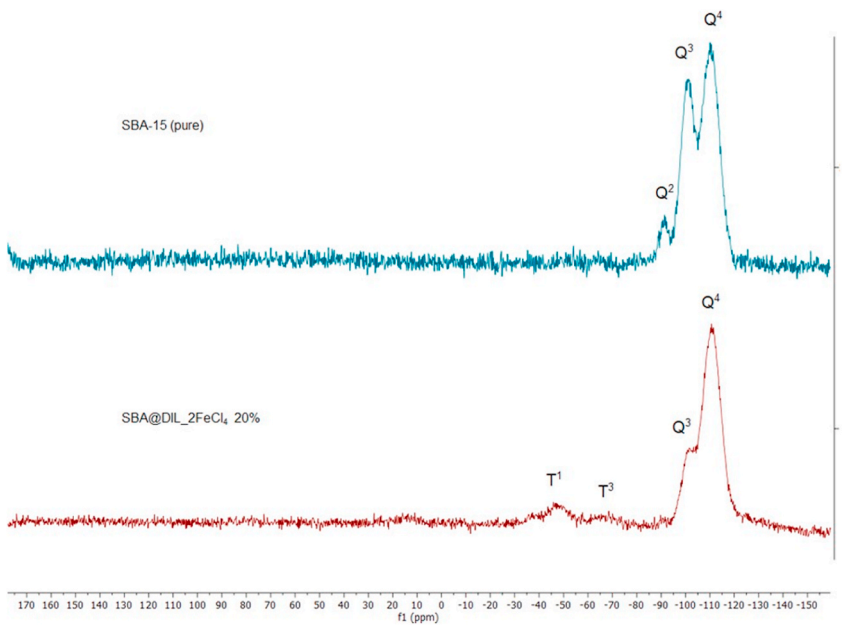

Fig. 8. ^{29}Si MAS-NMR spectra of SBA-15 (pure) and SBA@DIL_2Cl 20 %.

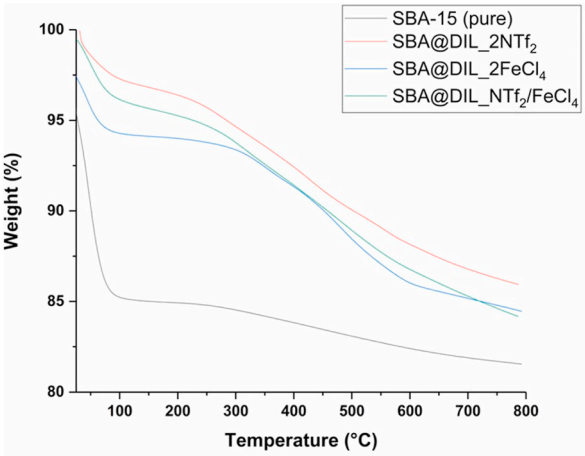

Fig. 9. Thermogravimetric analysis (TGA).

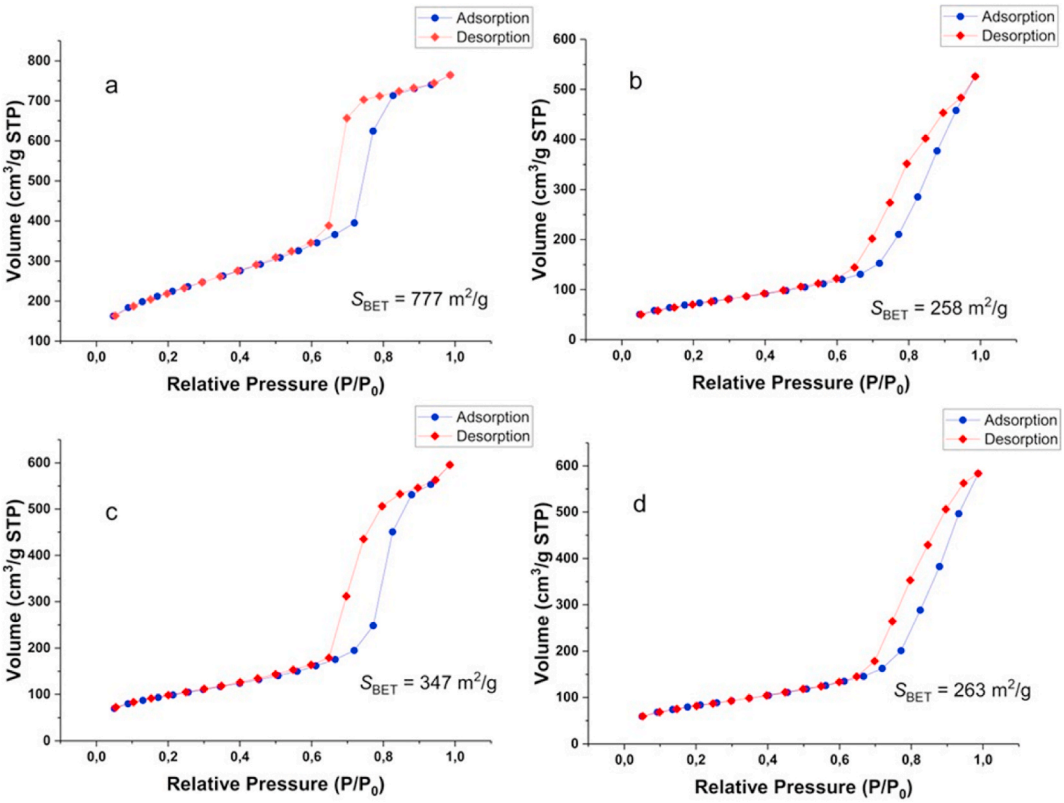

Fig. 10. Nitrogen adsorption/desorption BET isotherms at 77 K, for a) SBA-15 (pure), b) SBA@DIL_2NTf$_2$, c) SBA@DIL_2FeCl$_4$ e d) SBA@DIL_NTf$_2$/FeCl$_4$.

(263 m^2/g) and SAB@DIL_2NTf$_2$ (258 m^2/g)].

The pore size distribution and cumulative volume of SBA-15 and SBA-15 with immobilized DILs and MDILs were determined using the Barrett-Joyner-Halenda (BJH) model on isothermal adsorption data (Fig. 11). The results showed that the pore volume of the solid support decreased after immobilization with DILs and MDILs. The cumulative pore volume of SBA-15 was 1.021 cm^3/g, while it decreased to 0.802 cm^3/g for SBA@DIL_2NTf2, 0.899 cm^3/g for SBA@DIL_2FeCl$_4$, and 0.870 cm^3/g for SBA@DIL_NTf$_2$/FeCl$_4$. The average pore radius was calculated from the pore distribution curves and was found to be in the range of 4.216–5.366 nm.

The Raman spectra of the samples were analyzed as shown in Fig. 12. Only samples SBA@DIL_2FeCl$_4$ and SBA@DIL_NTf$_2$/FeCl$_4$ show peaks at 292 and 388 cm^{-1}, which are attributed to the symmetrical bending and stretching vibrations of the Cl–Fe–Cl bonds.

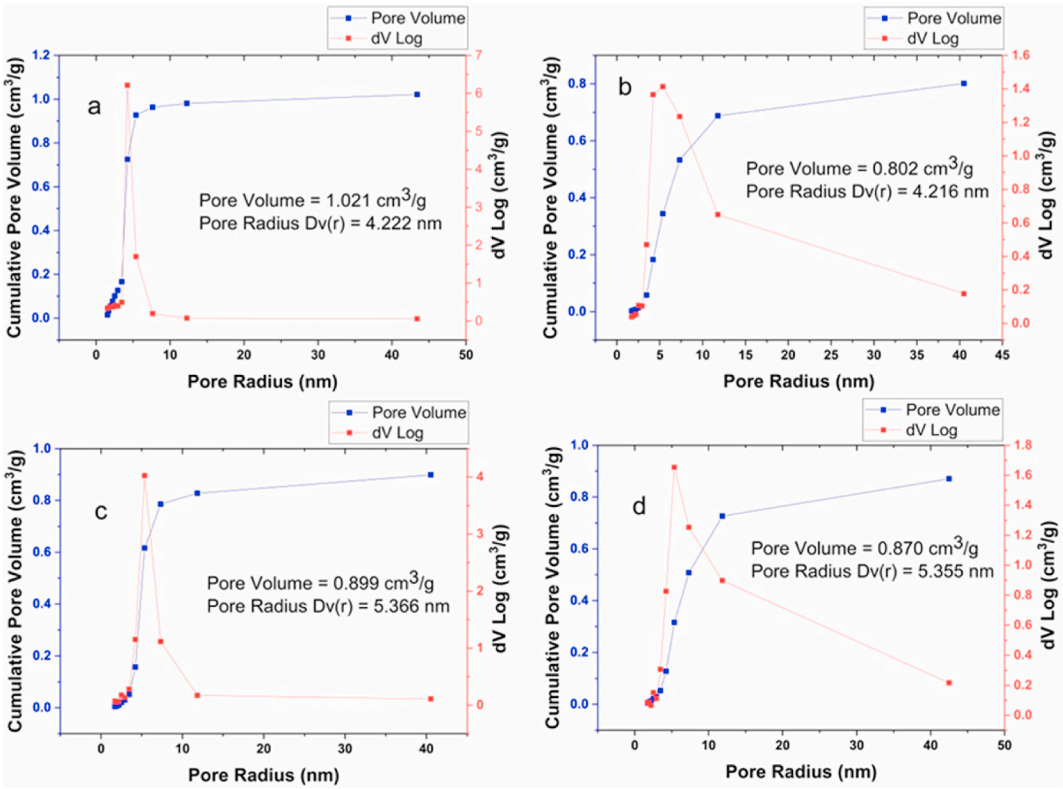

Fig. 11. BJH pore size distribution (red) and cumulative pore volume (blue) of the nitrogen isotherm at 77 K generated on a) SBA-15 (pure), b) SDIL_2NTf$_2$, c) SDIL_2FeCl$_4$, d) SDIL_NTf$_2$/FeCl$_4$.

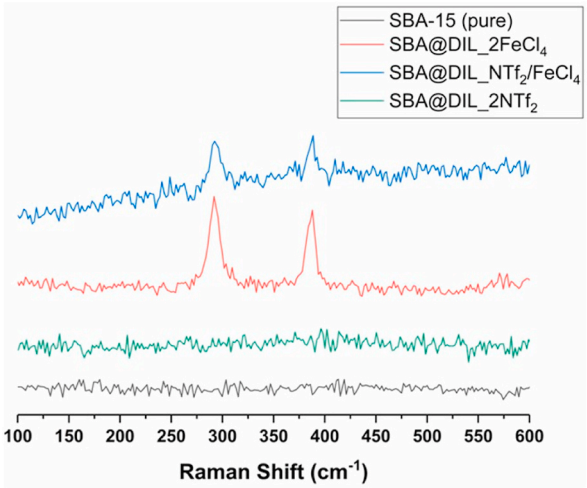

Fig. 12. Raman spectra of SBA-15 (pure), SBA@DIL_2NTf$_2$, SBA@DIL_2FeCl$_4$ and SBA@DIL_NTf$_2$/FeCl$_4$.

These peaks are characteristic of the $FeCl_4^-$ anionic complex. Table 1 compares the data obtained in this work with published studies, evidencing that the complex has been successfully formed.

The more intense peaks in SBA@DIL_2FeCl$_4$ than in SBA@DIL_NTf$_2$/FeCl$_4$ may be related to the greater amount of $FeCl_4^-$ anions present in the sample.

The SEM and TEM images of the samples are shown in Fig. 13. The pristine SBA-15 (see Fig. 13a) has a worm-like appearance in the form of cylindrical tubes composed of rope-like agglomerates of short rods as described in the literature [67]. Similar characteristics can be observed in their counterparts immobilized with ionic liquids. However, a slight alteration in surface morphology, such as

Table 1
Overview of the major peaks and assigned vibrations of the reference Raman spectra $FeCl_4^-$

Chemical specie	Peaks (cm^{-1})		References
$FeCl_4^-$	200	330	[63]
	134	334	[64]
	333	384	[65]
	333	384	[66]
	292	388	**This Work**

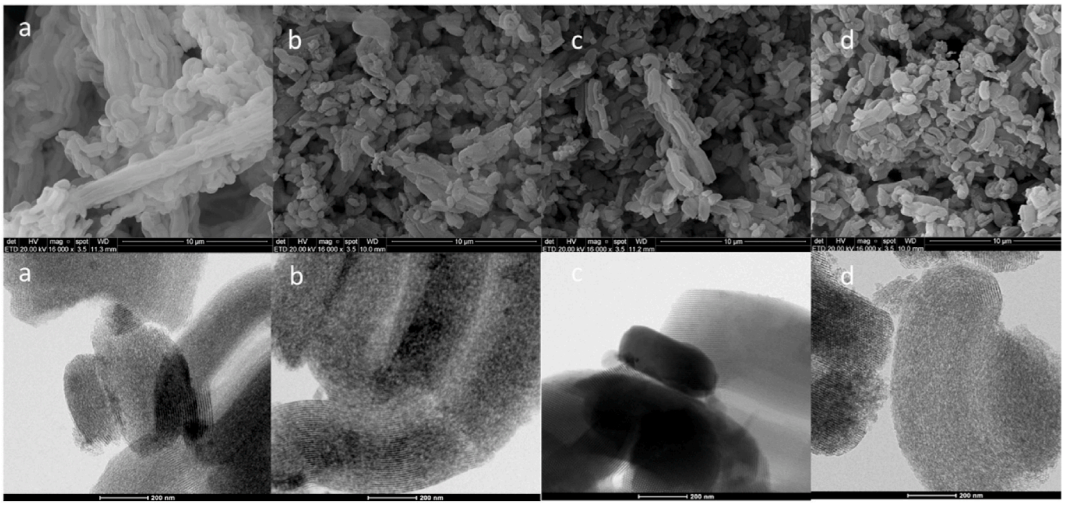

Fig. 13. SEM (10 μm) and TEM (200 nm) of a) SBA-15 (pure), b) SBA@DIL_2NTf$_2$, c) SBA@DIL_2FeCl$_4$ and d) SBA@DIL_NTf$_2$/FeCl$_4$.

reduced agglomeration of the rope-like aggregate, was observed on the immobilized supports, particularly those containing the NTf_2 anions, as depicted in Fig. 13 (b) and (d). This could be attributed to the immobilization of liquids, which does not solely occur within the pores. TEM images showed that the pore structures remained unchanged despite the slight morphological change.

The magnetic properties of the samples containing the anion $FeCl_4^-$ (SBA@DIL_2FeCl$_4$ and SBA@DIL_NTf$_2$/FeCl$_4$) were evaluated (see Fig. 14). The capability of an external magnetic field to influence materials containing this type of anion was analyzed. However, it was observed that it was not feasible to measure the response curves and generate the graphs $\boldsymbol{\delta M_R}$, indicating very weak magnetic interactions. This was attributed to the superposition of the diamagnetic signal from the samples themselves (SBA-15) and from the glass in the cylinder (sample holder).

Despite the ferromagnetic signal being superimposed on the diamagnetic signal, the SBA@DIL_2FeCl4 support shows a ferromagnetic signal 1.9 times greater than that of SBA@DIL_NTf$_2$/FeCl$_4$ (loops with coercivities of about 350 and 180 Oe). This indicates that the observed data was influenced by the 10 % (m/m) concentration of the ionic liquid.

3.3. CO_2 sorption and CO_2/N_2 selectivity tests

The CO_2 sorption performance of pristine SBA-15, supported DIL and MDILs can be seen in Fig. 15. In this type of material, the gas fills the pores, hence mesoporous supports with a high surface area tend to exhibit greater CO_2 sorption capacity, as observed in previous studies [50,56,68,69]. The data presented in Fig. 15 follow these characteristics, with the pristine SBA-15 showing the highest CO_2 capture capacity, followed by SBA@DIL_2FeCl$_4$ > SBA@DIL_NTf$_2$/FeCl$_4$ > SBA@DIL_2NTf$_2$. Consistent with the reduction in specific surface areas of the samples, fewer free pores result in lower CO_2 capture capacity. However, at the equilibrium pressure of 1 bar, it can be seen that pristine SBA-15 and SBA@DIL_2FeCl$_4$ have similar CO_2 sorption capacities, [58.61 (±4.48) $mgCO_2/g$] and [57.31 (±0.02) $mgCO_2/g$], respectively. This similarity is attributed to the fact that at higher pressures, CO_2 physisorption in the hexagonal pores of SBA-15 becomes the determining factor. The increase in CO_2 sorption at higher pressures is more strongly related to the available surface area and pore volume. Consequently, due to its lower porosity compared to unmodified silica supports, the CO_2 sorption of the grafted samples decreases, as reported by Mohamedali and coworkers [70]. This trend is evident from the behavior of the sorption curve when the pressures vary from 1 to 30 bar.

The CO_2/N_2 selectivity of the supports was evaluated (Fig. 16), with pristine SBA-15 showing the worst performance [3.22 (±0.45)], which can be attributed to its limited ability to interact with CO_2 molecules, primarily through interactions with the hydroxyls present on the support surface [71]. The support containing DIL with only NTf_2^- anions, SBA@DIL_2NTf$_2$, demonstrated an improvement in selectivity [9.92 (±0.72)], improving the selectivity of the material by approximately threefold. NTf_2^- is one of the most commonly used fluorinated anions for CO_2 capture, and the charge delocalization and low electrical polarizability resulting from

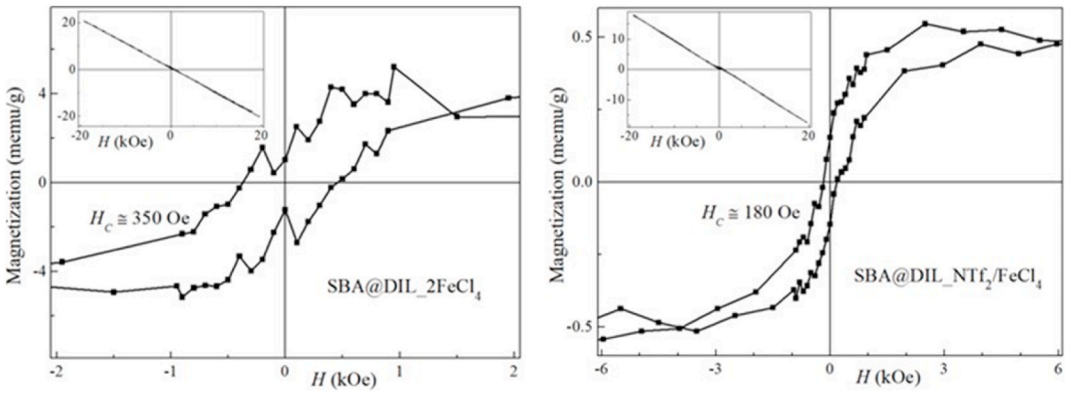

Fig. 14. Magnetization hysteresis loops of the SBA@DIL_2FeCl$_4$ and SBA@DIL_NTf$_2$/FeCl$_4$ samples. The insets show the row data in the whole magnetic-field range before performing diamagnetic correction.

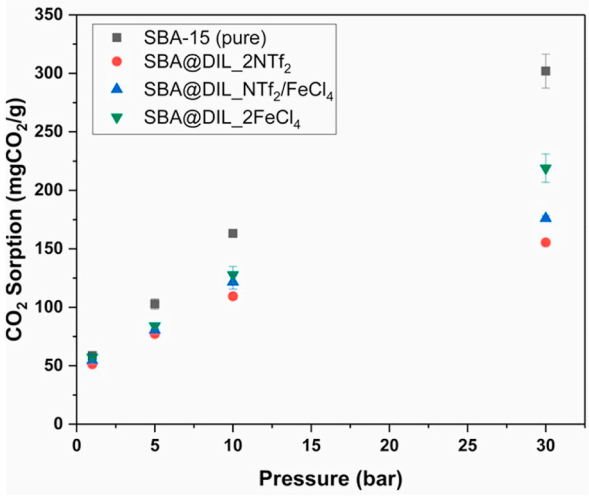

Fig. 15. CO_2 sorption at 25 °C at different pressures.

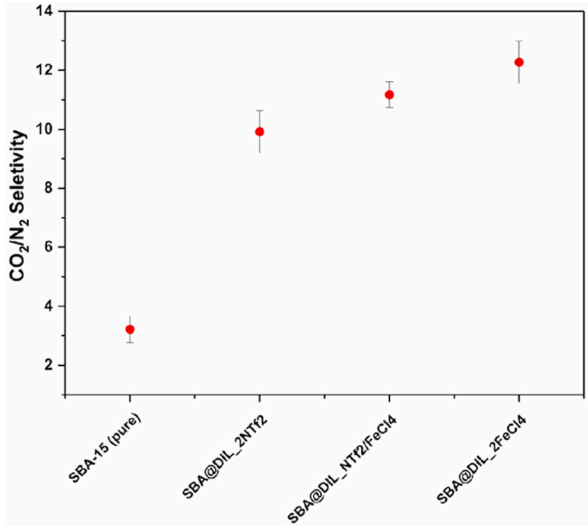

Fig. 16. CO_2/N_2 selectivities at 25 °C and 20 bar.

fluorination have corresponding effects on the electrostatic interactions and dispersion forces influencing CO_2 sorption, as noted by Zheng et al. [72]. However, fluorinated compounds are associated with high cost and negative environmental impact [73]. The mesoporous supports containing $FeCl_4$ anions performed most effectively in this study, with SBA@DIL_NTf_2/$FeCl_4$ [11.17 (±0.44)] and SBA@DIL_2$FeCl_4$ [12.27 (±0.72)] exhibiting notable performance. For the $FeCl_4$ anion, the interaction is attributed to coordination induced by metal ions, involving a coordination interaction between weakly electrophilic CO_2 and the metal center [74,75].

Although the effect of anions on CO_2 sorption is considered to be more significant than that of cations [76,77], the increased selectivity may also be related to the interactions between the imidazole cations and CO_2, including van der Waals forces, hydrogen bonding, and the steric effect of the imidazole cations [78,79]. In addition, the presence of an ether group as a ligand between the cations allows for Lewis acid-base interactions with CO_2 acting as a Lewis acid due to its low electron density compared to TEG [80,81]. This may explain the 3.8-fold increase in selectivity observed on the SBA@DIL_2$FeCl_4$ support.

Table 2 compares the CO_2 sorption and CO_2/N_2 selectivity results obtained in this work with those published in previous studies with mesoporous materials containing monocationic ionic liquids, impregnated and grafted with the same proportion of ionic liquid as in this study [10 %(w/w)], under conditions as close as possible. The data lead to the conclusion that the incorporation of MDILs into the SBA-15 support (SBA@DIL_NTf_2/$FeCl_4$ and SBA@DIL_2$FeCl_4$) shows a better CO_2/N_2 selectivity than the monocationic ionic liquids. This significant increase can be attributed to the greater number of coordination sites available [82], which doubles in the presence of two cations and two anions that have been shown to exhibit a strong interaction with CO_2. The use of the $FeCl_4$ anion, with its coordination interaction between the weakly electrophilic CO_2 and the metal center, outperformed the interaction promoted by the NTf_2 anion. The delocalization and the low electrical polarizability promoted by the fluorination have corresponding effects on the electrostatic interactions and dispersion forces influencing CO_2 absorption, as previously mentioned in the CO_2/N_2 selectivity. These factors contribute to the significant improvement, as illustrated in Table 2.

3.4. Stability tests

The stability test was carried out under the same conditions as the CO_2 capture capacity tests, with a selected equilibrium pressure of 10 bar, using the sample that showed the best CO_2 capture capacity and selectivity against CO_2/N_2, which was SBA@DIL_2$FeCl_4$. The sample underwent 10 sorption and desorption cycles, resulting in a consistent sorption value of [90.17 (±0.37)], as shown in Fig. 17.

The data allows us to conclude that both SBA-15, and MDIL (with $FeCl_4$ anion only) are stable. This suggests that chemically, the MDIL molecules and their active sites continue to facilitate the expected physisorption, while mechanically, the pores remain unaffected during retests. Enhancing competitiveness with aqueous amine solutions is intriguing, as it has the potential to lower process costs. Despite their affordability, aqueous amine solutions degrade over time due to chemisorption processes and exposure to high temperatures [14,87–89]. By utilizing less ionic liquid more efficiently, particularly through grafting onto supports, it could become more competitive. This approach, as suggested by Hiremath et al. [33] enhances adsorption kinetics and minimizes mass transfer resistance.

Table 2
CO_2 sorption and CO_2/N_2 selectivity, materials measured in this work compared to reported values in the literature.

			CO_2 sorption		Experimental Conditions			
Support	Funcionalization	Ionic Liquid	$mgCO_2/g$	mmol/g	P_{CO2}(bar)	T (°C)	CO_2/N_2 Selectivity	Ref.
Silica particles	Grafted	[P_{8883}]TFSI 10 %	–	0.99	1	40	6.0	[83]
ZIF-8	Impregnation	[Emim][Ac] 10 %	–	0.3	1	30	~7.5	[84]
Commercial Silica	Impregnation	mbmim[Tf_2N]10 %	52.1	–	4	45	6.9	[68]
Commercial Alumina	Impregnation	mbmim[Tf_2N]10 %	56.0	–	4	45	3.7	[68]
Commercial Silica	Grafted	[i-C_5TPIm][Cl] 10 %	60.68	–	4	45	4.34	[56]
Commercial Silica	Grafted	[i-C_5TPIm][Tf_2N] 10 %	69.38	–	4	45	4.38	[56]
Activated Carbon	Impregnation	[bmpy][Tf_2N] 10 %	–	0.62	1	25	–	[85]
SiO_2	Grafted	[bmim][CF_3SO_3] 10 %	11.90	–	1	25	–	[86]
SBA-15	Grafted	DIL_2$FeCl_4$ 10 %	57.30	1.30	1	25	12.3	**This work**
SBA-15	Grafted	DIL_NTf_2/$FeCl_4$ 10 %	54.42	1.24	1	25	11.2	**This work**
SBA-15	Grafted	DIL_2$FeCl_4$ 10 %	90.33	2.05	5	25	12.3	**This work**
SBA-15	Grafted	DIL_NTf_2/$FeCl_4$ 10 %	80.48	1.83	5	25	11.2	**This work**

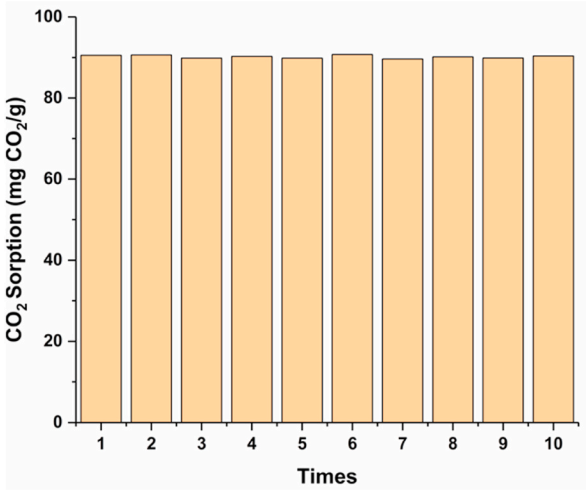

Fig. 17. CO_2 sorption/dessorption tests on SBA@DIL_2$FeCl_4$ (25 °C; 5 bar).

4. Conclusion

To expand the options for CO_2 capture and separation, we developed imidazolium-based dicationic ionic liquids (DILs) linked by TEG and combined with different anions ($2NTf_2$, $2FeCl_4$ and $NTf_2/FeCl_4$). The DILs were successfully supported in the SBA-15 10 % (w/w). MDIL with $FeCl_4$ anion presented the best results both for CO_2 sorption and CO_2/N_2 separation compared to fluorinated anions. Yet, SBA@DIL_2$FeCl_4$ proved to be chemically and mechanically stable, making it a promising option for use in post-combustion processes.

Compared to the results obtained with monocationic ionic liquids described in the literature using mesoporous supports and the same percentage of IL content, our results show that the use of DILs leads to improved CO_2 capture and selectivity due to increased availability of coordination sites.

CRediT authorship contribution statement

Evandro Duarte: Writing – original draft, Methodology, Data curation. **Franciele Bernard:** Validation, Methodology, Formal analysis, Conceptualization. **Leonardo Moreira Dos Santos:** Validation, Resources, Methodology, Data curation. **Barbara B. Polesso:** Methodology, Validation. **Rafael Duczinski:** Methodology, Formal analysis, Conceptualization. **Vitor Forneck:** Methodology, Formal analysis. **Julian Geshev:** Methodology, Formal analysis. **Sandra Einloft:** Writing – review & editing, Writing – original draft, Validation, Supervision, Resources, Project administration, Funding acquisition, Conceptualization.

Declaration of competing interest

The authors declare that they have no known competing financial interests or personal relationships that could have appeared to influence the work reported in this paper.

Acknowledgments

This work was supported by the Coordenação de Aperfeiçoamento de Pessoal de Nivel Superior – Brasil (CAPES) – Finance Code 001 and CNPq through a PQ grant.

References

[1] United Nations, “What Is Climate Change? | United Nations”, Accessed: January. 28, 2022. [Online]. Available: https://www.un.org/en/climatechange/what-is-climate-change.
[2] WORLD METEOROLOGICAL ORGANIZATION, “WMO ATLAS OF MORTALITY AND ECONOMIC LOSSES FROM WEATHER, CLIMATE AND WATER EXTREMES (1970–2019).” Accessed: July. 5, 2022. [Online]. Available: https://library.wmo.int/doc_num.php?explnum_id=10989.
[3] WORLD METEOROLOGICAL ORGANIZATION, State of the Global Climate 2021, 2022.
[4] Climatewatch, “Climate Watch Historical Country Greenhouse Gas Emissions Data (1990-2018).” Accessed: March. 2, 2022. [Online]. Available: https://www.climatewatchdata.org/ghg-emissions?breakBy=gas&chartType=area&end_year=2018&start_year=1990.
[5] IPCC, “Climate Change 2022: Mitigation of Climate Change.” Accessed: July. 5, 2022. [Online]. Available: https://report.ipcc.ch/ar6wg3/pdf/IPCC_AR6_WGIII_FinalDraft_FullReport.pdf.
[6] NOAA, Carbon dioxide now more than 50% higher than pre-industrial levels | National Oceanic and Atmospheric Administration [Online]. Available: https://www.noaa.gov/news-release/carbon-dioxide-now-more-than-50-higher-than-pre-industrial-levels, 2022. (Accessed 12 June 2022).

[7] NOAA, "Climate Change: Atmospheric Carbon Dioxide." Accessed: February. 5, 2022. [Online]. Available: https://www.climate.gov/news-features/understanding-climate/climate-change-atmospheric-carbon-dioxide.

[8] A. Al-Mamoori, A. Krishnamurthy, A.A. Rownaghi, F. Rezaei, Carbon capture and utilization Update, Energy Technol. 5 (6) (2017) 834–849, https://doi.org/10.1002/ente.201600747.

[9] I. Ghiat, T. Al-Ansari, A review of carbon capture and utilisation as a CO2 abatement opportunity within the EWF nexus, J. CO2 Util. 45 (Mar. 2021) 101432, https://doi.org/10.1016/J.JCOU.2020.101432.

[10] J.D. Figueroa, T. Fout, S. Plasynski, H. McIlvried, R.D. Srivastava, Advances in CO2 capture technology—the U.S. Department of Energy's carbon Sequestration program, Int. J. Greenh. Gas Control 2 (1) (Jan. 2008) 9–20, https://doi.org/10.1016/S1750-5836(07)00094-1.

[11] O. Akeeb, L. Wang, W. Xie, R. Davis, M. Alkasrawi, S. Toan, Post-combustion CO2 capture via a variety of temperature ranges and material adsorption process: a review, J. Environ. Manag. 313 (Jul. 2022) 115026, https://doi.org/10.1016/J.JENVMAN.2022.115026.

[12] S.Y. Oh, M. Binns, H. Cho, J.K. Kim, Energy minimization of MEA-based CO2 capture process, Appl. Energy 169 (May 2016) 353–362, https://doi.org/10.1016/J.APENERGY.2016.02.046.

[13] N. Wang, Z. Peng, H. Gao, T. Sema, J. Shi, Z. Liang, New insight and evaluation of secondary Amine/N-butanol biphasic solutions for CO2 Capture: equilibrium Solubility, phase separation Behavior, absorption Rate, desorption Rate, energy consumption and ion species, Chem. Eng. J. 431 (Mar. 2022) 133912, https://doi.org/10.1016/J.CEJ.2021.133912.

[14] A. Mukherjee, J.A. Okolie, A. Abdelrasoul, C. Niu, A.K. Dalai, Review of post-combustion carbon dioxide capture technologies using activated carbon, J. Environ. Sci. 83 (Sep. 2019) 46–63, https://doi.org/10.1016/J.JES.2019.03.014.

[15] Z. Shamair, N. Habib, M.A. Gilani, A.L. Khan, Theoretical and experimental investigation of CO2 separation from CH4 and N2 through supported ionic liquid membranes, Appl. Energy 268 (Jun. 2020) 115016, https://doi.org/10.1016/J.APENERGY.2020.115016.

[16] I. Yasmeen, et al., Synergistic effects of highly selective ionic liquid confined in nanocages: exploiting the three component mixed matrix membranes for CO2 capture, Chem. Eng. Res. Des. 155 (Mar. 2020) 123–132, https://doi.org/10.1016/J.CHERD.2020.01.006.

[17] A. Ilyas, N. Muhammad, M.A. Gilani, K. Ayub, I.F.J. Vankelecom, A.L. Khan, Supported protic ionic liquid membrane based on 3-(trimethoxysilyl)propan-1-aminium acetate for the highly selective separation of CO2, J. Memb. Sci. 543 (Dec. 2017) 301–309, https://doi.org/10.1016/J.MEMSCI.2017.08.071.

[18] V. Indira, K. Abhitha, A review on recent developments in Zeolite A synthesis for improved carbon dioxide capture: implications for the water-energy nexus, Energy Nexus 7 (Sep. 2022) 100095, https://doi.org/10.1016/J.NEXUS.2022.100095.

[19] D.G. Boer, J. Langerak, P.P. Pescarmona, Zeolites as selective adsorbents for CO2 separation, ACS Appl. Energy Mater. 6 (5) (Mar. 2023) 2634–2656, https://doi.org/10.1021/ACSAEM.2C03605/ASSET/IMAGES/LARGE/AE2C03605_0014.JPEG.

[20] S. Kumar, R. Srivastava, J. Koh, Utilization of zeolites as CO2 capturing agents: advances and future perspectives, J. CO2 Util. 41 (Oct. 2020) 101251, https://doi.org/10.1016/J.JCOU.2020.101251.

[21] A. Policicchio, et al., Hexagonal mesoporous silica for carbon capture: unrevealing CO2 microscopic dynamics by nuclear magnetic resonance, J. CO2 Util. 55 (Jan. 2022) 101809, https://doi.org/10.1016/J.JCOU.2021.101809.

[22] M. Ravutsov, Y. Mitrev, P. Shestakova, H. Lazarova, S. Simeonov, M. Popova, Co2 adsorption on modified mesoporous silicas: the role of the adsorption sites, Nanomaterials 11 (11) (Nov. 2021), https://doi.org/10.3390/NANO11112831/S1.

[23] O. Tumurbaatar, M. Popova, V. Mitova, P. Shestakova, N. Koseva, Engineering of silica mesoporous materials for CO2 adsorption, Materials 16 (11) (Jun. 2023) 4179, https://doi.org/10.3390/MA16114179/S1.

[24] M.G. Plaza, A.S. González, C. Pevida, J.J. Pis, F. Rubiera, Valorisation of spent coffee grounds as CO2 adsorbents for postcombustion capture applications, Appl. Energy 99 (Nov. 2012) 272–279, https://doi.org/10.1016/J.APENERGY.2012.05.028.

[25] N. Abuelnoor, A. AlHajaj, M. Khaleel, L.F. Vega, M.R.M. Abu-Zahra, Activated carbons from biomass-based sources for CO2 capture applications, Chemosphere 282 (Nov. 2021) 131111, https://doi.org/10.1016/J.CHEMOSPHERE.2021.131111.

[26] S. Acevedo, L. Giraldo, J.C. Moreno-Piraján, Adsorption of CO2 on activated carbons prepared by chemical activation with cupric nitrate, ACS Omega 5 (18) (May 2020) 10423–10432, https://doi.org/10.1021/ACSOMEGA.0C00342/ASSET/IMAGES/LARGE/AO0C00342_0005.JPEG.

[27] P. Zhao, G. Zhang, H. Yan, Y. Zhao, The latest development on amine functionalized solid adsorbents for post-combustion CO2 capture: analysis review, Chin. J. Chem. Eng. 35 (Jul. 2021) 17–43, https://doi.org/10.1016/J.CJCHE.2020.11.028.

[28] P. Zhao, Y. Yin, W. Cheng, X. Xu, D. Yang, W. Yuan, Development of facile synthesized mesoporous carbon composite adsorbent for efficient CO2 capture, J. CO2 Util. 50 (Aug. 2021) 101612, https://doi.org/10.1016/J.JCOU.2021.101612.

[29] N.A. Rashidi, S. Yusup, An overview of activated carbons utilization for the post-combustion carbon dioxide capture, J. CO2 Util. 13 (Mar. 2016) 1–16, https://doi.org/10.1016/J.JCOU.2015.11.002.

[30] J. Zhang, et al., Preparation of mesoporous coal-gasification fine slag adsorbent via amine modification and applications in CO2 capture, Appl. Surf. Sci. 537 (Jan. 2021) 147938, https://doi.org/10.1016/J.APSUSC.2020.147938.

[31] A. Berthod, M.J. Ruiz-Ángel, S. Carda-Broch, Recent advances on ionic liquid uses in separation techniques, J. Chromatogr. A 1559 (Jul. 20, 2018) 2–16, https://doi.org/10.1016/j.chroma.2017.09.044.

[32] S. Zeng, et al., Ionic-liquid-based CO2 capture systems: structure, interaction and process, Chem. Rev. 117 (14) (Jul. 2017) 9625–9673, https://doi.org/10.1021/ACS.CHEMREV.7B00072.

[33] V. Hiremath, A.H. Jadhav, H. Lee, S. Kwon, J.G. Seo, Highly reversible CO2 capture using amino acid functionalized ionic liquids immobilized on mesoporous silica, Chem. Eng. J. 287 (Mar. 2016) 602–617, https://doi.org/10.1016/J.CEJ.2015.11.075.

[34] A.O. Ezzat, A.M. Atta, H.A. Al-Lohedan, Demulsification of stable seawater/Arabian heavy crude oil emulsions using star-like tricationic pyridinium ionic liquids, Fuel 304 (Nov. 2021) 121436, https://doi.org/10.1016/J.FUEL.2021.121436.

[35] L. Qiao, X. Shi, X. Lu, G. Xu, Preparation and evaluation of surface-bonded tricationic ionic liquid silica as stationary phases for high-performance liquid chromatography, J. Chromatogr. A 1396 (May 2015) 62–71, https://doi.org/10.1016/j.chroma.2015.03.081.

[36] Arjun Kumbhar, Sanjay Jadhav, Rajendra Shejwal, Gajanan Rashinkar, Rajshri Salunkhe, Application of novel multi-cationic ionic liquids in microwave assisted 2-amino-4 H -chromene synthesis, RSC Adv. 6 (23) (Feb. 2016) 19612–19619, https://doi.org/10.1039/C6RA01062H.

[37] R. Pan, Y. Guo, Y. Tang, D. Wei, L. Mengli, D. He, Dicationic liquid containing alkenyl modified CuBTC improves the performance of the composites: increasing the CO2 adsorption effect, Chem. Eng. J. 430 (Feb. 2022) 132127, https://doi.org/10.1016/J.CEJ.2021.132127.

[38] A. Hafizi, M. Rajabzadeh, M.H. Mokari, R. Khalifeh, Synthesis, property analysis and absorption efficiency of newly prepared tricationic ionic liquids for CO2 capture, J. Mol. Liq. 324 (Feb. 2021) 115108, https://doi.org/10.1016/j.molliq.2020.115108.

[39] S. Li, W. Zhao, G. Feng, P.T. Cummings, A computational study of dicationic ionic liquids/co2 interfaces, Langmuir 31 (8) (Mar. 2015) 2447–2454, https://doi.org/10.1021/LA5048563/SUPPL_FILE/LA5048563_SI_001.

[40] Y. Zhang, P. Yu, Y. Luo, Absorption of CO2 by amino acid-functionalized and traditional dicationic ionic liquids: properties, Henry's law constants and mechanisms, Chem. Eng. J. 214 (Jan. 2013) 355–363, https://doi.org/10.1016/j.cej.2012.10.080.

[41] M.M. Cruz, et al., Thermophysical and magnetic studies of two paramagnetic liquid salts: [C4mim][FeCl4] and [P66614][FeCl4], Fluid Phase Equil. 350 (Jul. 2013) 43–50, https://doi.org/10.1016/j.fluid.2013.03.001.

[42] J. Albo, et al., Separation performance of CO2 through supported magnetic ionic liquid membranes (SMILMs), Sep. Purif. Technol. 97 (Sep. 2012) 26–33, https://doi.org/10.1016/J.SEPPUR.2012.01.034.

[43] E. Santos, J. Albo, C.I. Daniel, C.A.M. Portugal, J.G. Crespo, A. Irabien, Permeability modulation of supported magnetic ionic liquid membranes (SMILMs) by an external magnetic field, J. Memb. Sci. 430 (Mar. 2013) 56–61, https://doi.org/10.1016/j.memsci.2012.12.009.

[44] W. Shan et al., "A New Class of Type III Porous Liquids: A Promising Platform for Rational Adjustment of Gas Sorption Behavior.".

[45] Y. Wang, C. Yue, X. Li, J. Luo, Synthesis of a novel poly(ethylene glycol) grafted triethylamine functionalized dicationic ionic liquid and its application in one-pot synthesis of 2-amino-2-chromene derivatives in water, Compt. Rendus Chem. 19 (8) (Aug. 2016) 1021–1026, https://doi.org/10.1016/J.CRCI.2016.03.002.

[46] M.K. Dinker, P.S. Kulkarni, Insight into the PEG-linked bis-imidazolium bridged framework of mesoporous organosilicas as ion exchangers, Microporous Mesoporous Mater. 230 (2016) 145–153, https://doi.org/10.1016/J.MICROMESO.2016.05.008.

[47] S. Magalhães, et al., Brief overview on bio-based adhesives and sealants, Polym. 2019 11 (10) (Oct. 2019) 1685, https://doi.org/10.3390/POLYM11101685.

[48] A.S. Aquino, et al., Rationalizing the role of the anion in CO2 capture and conversion using imidazolium-based ionic liquid modified mesoporous silica, RSC Adv. 5 (79) (Jul. 2015) 64220–64227, https://doi.org/10.1039/C5RA07561K.

[49] Y.L. Hu, Preparation of silica supported ionic liquids for highly selective hydroxylation of aromatics with hydrogen peroxide under solvent-free conditions [Online]. Available: http://www.scielo.org.mx/scielo.php?script=sci_arttext&pid=S1870-249X2016000400207#ch3, 2016. (Accessed 6 June 2022).

[50] B.B. Polesso, F.L. Bernard, H.Z. Ferrari, E.A. Duarte, F.D. Vecchia, S. Einloft, Supported ionic liquids as highly efficient and low-cost material for CO_2/CH_4 separation process, Heliyon 5 (7) (2019) e02183, https://doi.org/10.1016/j.heliyon.2019.e02183.

[51] W.J. Koros, D.R. Paul, Design considerations for measurement of gas sorption in polymers by pressure decay, J. Polym. Sci. Polym. Phys. Ed. 14 (10) (Oct. 1976) 1903–1907, https://doi.org/10.1002/POL.1976.180141014.

[52] M. Fernández Rojas, et al., New biocomposites based on castor oil polyurethane foams and ionic liquids for CO2 capture, Fluid Phase Equil. 452 (Nov. 2017) 103–112, https://doi.org/10.1016/J.FLUID.2017.08.026.

[53] F.L. Bernard, et al., Cellulose based poly(ionic liquids): tuning cation-anion interaction to improve carbon dioxide sorption, Fuel 211 (Jan. 2018) 76–86, https://doi.org/10.1016/J.FUEL.2017.09.057.

[54] A. Azimi, M. Mirzaei, Experimental evaluation and thermodynamic modeling of hydrate selectivity in separation of CO2 and CH4, Chem. Eng. Res. Des. 111 (Jul. 2016) 262–268, https://doi.org/10.1016/J.CHERD.2016.05.005.

[55] M. Ates, N. Uludag, T. Karazehir, Copolymer formation of 9-(2-(benzyloxy)ethyl)-9H-carbazole and 1-tosyl-1H-pyrrole coated on glassy carbon electrode and electrochemical impedance spectroscopy, J. Solid State Electrochem. 16 (8) (Aug. 2012) 2639–2649, https://doi.org/10.1007/S10008-012-1688-5.

[56] R. Duczinski, et al., Enhancement of CO2/N2 selectivity and CO2 uptake by tuning concentration and chemical structure of imidazolium-based ILs immobilized in mesoporous silica, J. Environ. Chem. Eng. 8 (3) (Jun. 2020) 103740, https://doi.org/10.1016/J.JECE.2020.103740.

[57] G. Zante, et al., Grafted mesoporous silicas for radionuclide uptake: radiolytic stability under electron irradiation, Microporous Mesoporous Mater. 336 (May 2022) 111851, https://doi.org/10.1016/J.MICROMESO.2022.111851.

[58] E.P.F. Nhavene, G.F. Andrade, J.A.Q. Arantes Faria, D.A. Gomes, E.M.B. de Sousa, Biodegradable polymers grafted onto multifunctional mesoporous silica nanoparticles for gene delivery, ChemEngineering 2 (2) (May 2018) 24, https://doi.org/10.3390/CHEMENGINEERING2020024, 2018, Vol. 2, Page 24.

[59] J. McElwee, R. Helmy, A.Y. Fadeev, Thermal stability of organic monolayers chemically grafted to minerals, J. Colloid Interface Sci. 285 (2) (May 2005) 551–556, https://doi.org/10.1016/J.JCIS.2004.12.006.

[60] Y. Sánchez-Vicente, C. Pando, M. Cortijo, A. Cabañas, Chemical surface modification of mesoporous silica SBA-15 with a tertiary aminosilane using supercritical carbon dioxide, Microporous Mesoporous Mater. 193 (Jul. 2014) 145–153, https://doi.org/10.1016/J.MICROMESO.2014.03.021.

[61] K.S.W. Rouquerol, Rouquerol Jean, Françoise; Llewellyn, Philip ; Maurin, Guillaume; Sing, Adsorption by Powders and Porous Solids: Principles, Methodology and Application, second ed., Academic Press, 1999 [Online]. Available: https://books.google.com.br/books?hl=en&lr=&id=UOE-ZscCYncC&oi=fnd&pg=PP1&ots=0T-TICskjx&sig=SGufVZYmAnBWGCXiPTkm5zowILc&redir_esc=y#v=onepage&q=hysteresis&f=false. (Accessed 19 December 2022).

[62] K.S.W. Sing, et al., Reporting physisorption data for gas/solid systems with special reference to the determination of surface area and porosity, Pure Appl. Chem. 57 (4) (Jan. 1985) 603–619, https://doi.org/10.1351/PAC198557040603/MACHINEREADABLECITATION/RIS.

[63] Y. Kemmizaki, Y. Katayama, H. Tsutsumi, K. Ueno, Redox-active glyme-li tetrahalogenoferrate(III) solvate ionic liquids for semi-liquid lithium secondary batteries, RSC Adv. 10 (7) (2020) 4129–4136, https://doi.org/10.1039/C9RA10149G.

[64] X. Yu, X. Yuan, Y. Zhao, L. Ren, From paramagnetic to superparamagnetic ionic liquid/poly(ionic liquid): the effect of π-πStacking interaction, ACS Macro Lett. 8 (2019) 1504–1510, https://doi.org/10.1021/ACSMACROLETT.9B00714/ASSET/IMAGES/LARGE/MZ9B00714_0004.JPEG.

[65] J.G. Li, Y.F. Hu, S.F. Sun, S. Ling, J.Z. Zhang, Ionic structures of nanobased FeCl3/[C4mim]Cl ionic liquids, J. Phys. Chem. B 116 (22) (Jun. 2012) 6461–6464, https://doi.org/10.1021/JP206819H/ASSET/IMAGES/LARGE/JP-2011-06819H_0007.JPEG.

[66] M.S. Sitze, E.R. Schreiter, E.V. Patterson, R.G. Freeman, Ionic liquids based on FeCl3 and FeCl2. Raman scattering and ab initio calculations, Inorg. Chem. 40 (10) (May 2001) 2298–2304, https://doi.org/10.1021/IC001042R/SUPPL_FILE/IC001042R_S.PDF.

[67] D. Zhao, Q. Huo, J. Feng, B.F. Chmelka, G.D. Stucky, Nonionic triblock and star diblock copolymer and oligomeric sufactant syntheses of highly ordered, hydrothermally stable, mesoporous silica structures, J. Am. Chem. Soc. 120 (24) (1998) 6024–6036, https://doi.org/10.1021/JA974025I/SUPPL_FILE/JA6024.PDF.

[68] B. B. Polesso et al., "Imidazolium-based Ionic Liquids Impregnated in Silica and Alumina Supports for CO 2 Capture", doi: 10.1590/1980-5373-MR-2018-0810..

[69] R. Duczinski, et al., Waste derived MCMRH- supported IL for CO2/CH4 separation, J. Nat. Gas Sci. Eng. 54 (Jun. 2018) 54–64, https://doi.org/10.1016/J.JNGSE.2018.03.028.

[70] M. Mohamedali, H. Ibrahim, A. Henni, Imidazolium based ionic liquids confined into mesoporous silica MCM-41 and SBA-15 for carbon dioxide capture, Microporous Mesoporous Mater. 294 (2020) 109916, https://doi.org/10.1016/J.MICROMESO.2019.109916.

[71] R.R.D.J.N. Subagyono, A.L. Chaffee, CO2 adsorption on SBA-15: a molecular modelling, IOP Conf. Ser. Earth Environ. Sci. 144 (1) (Apr. 2018) 012045, https://doi.org/10.1088/1755-1315/144/1/012045.

[72] X. Zheng, et al., Understanding the interactions between the bis(trifluoromethylsulfonyl)imide anion and absorbed CO2 using X-ray diffraction analysis of a soft crystal surrogate, Commun. Chem. 3 (1) (Oct. 2020) 1–7, https://doi.org/10.1038/s42004-020-00390-1, 2020 31.

[73] H. Zhao, G.A. Baker, Functionalized ionic liquids for CO2 capture under ambient pressure, Green Chem. Lett. Rev. 16 (1) (Jan. 2023), https://doi.org/10.1080/17518253.2022.2149280.

[74] B. Li, C. Wang, Y. Zhang, Y. Wang, High CO2 absorption capacity of metal-based ionic liquids: a molecular dynamics study, Green Energy Environ. 6 (2) (Apr. 2021) 253–260, https://doi.org/10.1016/J.GEE.2020.04.009.

[75] T. Zhang, et al., Theoretical insights into the depolymerization mechanism of lignin to methyl p-hydroxycinnamate by [Bmim][FeCl4] ionic liquid, Front. Chem. 7 (JUN) (2019) 446, https://doi.org/10.3389/FCHEM.2019.00446/FULL.

[76] J.L. Anthony, J.L. Anderson, E.J. Maginn, J.F. Brennecke, Anion Effects on Gas Solubility in Ionic Liquids, 2005, https://doi.org/10.1021/jp046404l.

[77] O. Yuksel Orhan, Effects of various anions and cations in ionic liquids on CO2 capture, J. Mol. Liq. 333 (Jul. 2021) 115981, https://doi.org/10.1016/J.MOLLIQ.2021.115981.

[78] M. Prakash, K. Mathivon, D.M. Benoit, G. Chambaud, M. Hochlaf, Carbon dioxide interaction with isolated imidazole or attached on gold clusters and surface: competition between σ H-bond and π stacking interaction, Phys. Chem. Chem. Phys. 16 (24) (May 2014) 12503–12509, https://doi.org/10.1039/C4CP01292E.

[79] M. Salah, K. Marakchi, S. Dalbouha, M.L. Senent, O.K. Kabbaj, N. Komiha, Influence of the functionalization of imidazole on its CO2 uptake efficiency. A theoretical contribution, Comput. Theor. Chem. 1073 (Dec. 2015) 1–8, https://doi.org/10.1016/J.COMPTC.2015.09.010.

[80] B.S. Lee, Effect of specific interaction of CO2 with poly(ethylene glycol) on phase behavior, J. CO2 Util. 28 (Dec. 2018) 228–234, https://doi.org/10.1016/J.JCOU.2018.10.002.

[81] C.L. Bentley, T. Song, B.J. Pedretti, M.J. Lubben, N.A. Lynd, J.F. Brennecke, Effects of poly(glycidyl ether) structure and ether oxygen placement on CO2Solubility, J. Chem. Eng. Data 66 (7) (Jul. 2021) 2832–2843, https://doi.org/10.1021/ACS.JCED.1C00219/ASSET/IMAGES/LARGE/JE1C00219_0008.JPEG.

[82] S.D. Hojniak, et al., Separation of carbon dioxide from nitrogen or methane by supported ionic liquid membranes (SILMs): influence of the cation charge of the ionic liquid, J. Phys. Chem. B 117 (48) (Dec. 2013) 15131–15140, https://doi.org/10.1021/JP409414T.

[83] J. Zhu, B. He, J. Huang, C. Li, T. Ren, Effect of immobilization methods and the pore structure on CO2 separation performance in silica-supported ionic liquids, Microporous Mesoporous Mater. 260 (Apr. 2018) 190–200, https://doi.org/10.1016/J.MICROMESO.2017.10.035.

[84] M. Mohamedali, H. Ibrahim, A. Henni, Incorporation of acetate-based ionic liquids into a zeolitic imidazolate framework (ZIF-8) as efficient sorbents for carbon dioxide capture, Chem. Eng. J. 334 (Feb. 2018) 817–828, https://doi.org/10.1016/J.CEJ.2017.10.104.

[85] S.S. Fatima, A. Borhan, M. Ayoub, N.A. Ghani, CO2 adsorption performance on surface-functionalized activated carbon impregnated with pyrrolidinium-based ionic liquid, Process 10 (11) (Nov. 2022) 2372, https://doi.org/10.3390/PR10112372, 2022, Vol. 10, Page 2372.
[86] T.S. Marliza, M.A. Yarmo, A.H. Lahuri, Y.H. Taufiq-Yap, CO2 capture using ionic liquid hybrid sorbent: physical and chemical adsorption-desorption study, Mater. Today Proc. 64 (Jan. 2022) 20–26, https://doi.org/10.1016/J.MATPR.2022.03.471.
[87] C. Gouedard, D. Picq, F. Launay, P.L. Carrette, Amine degradation in CO2 capture. I. A review, Int. J. Greenh. Gas Control 10 (Sep. 2012) 244–270, https://doi.org/10.1016/J.IJGGC.2012.06.015.
[88] A. Azarpour, S. Zendehboudi, Hybrid smart strategies to predict amine thermal degradationin industrial CO2 capture processes, ACS Omega 8 (30) (Aug. 2023) 26850, https://doi.org/10.1021/ACSOMEGA.3C01475.
[89] S. Delgado, B. Valentin, D. Bontemps, O. Authier, Degradation of amine solvents in a CO2 capture plant at lab-scale: experiments and modeling, Ind. Eng. Chem. Res. 57 (18) (May 2018) 6057–6067, https://doi.org/10.1021/ACS.IECR.7B05225/ASSET/IMAGES/LARGE/IE-2017-05225B_0006.JPEG.